

The following publication Chow, R., Mok, D.K.W., Lee, E.P.F., & Dyke, J.M. (2021). Comment on “Impact of water on the BrO + HO₂ gas-phase reaction: mechanism, kinetics and products” by N. T. Tsona, S. Tang and L. Du, Phys. Chem. Chem. Phys., 2019, 21, 20296. Physical Chemistry Chemical Physics, 23(10), 6309-6315 is available at <https://doi.org/10.1039/d0cp00222d>.

Comment on

“Impact of water on the BrO + HO₂ gas-phase reaction: mechanism, kinetics and products” by Tsona et al. PCCP 2019, 21, 20296-20307

by

Ronald Chow ^[a], Daniel K.W. Mok ^[a], Edmond P. F. Lee ^{*[a],[b]}, and John M. Dyke ^{*[b]}

^[a] Department of Applied Biology and Chemical Technology, Hong Kong Polytechnic University, Hung Hom, Hong Kong

^[b] School of Chemistry, University of Southampton, Highfield, Southampton SO17 1BJ, United Kingdom e-mail epl@soton.ac.uk; jmdyke@soton.ac.uk

*addresses for correspondence

Abstract

The reaction, $\text{BrO} + \text{HO}_2 \rightarrow \text{HOBr} + \text{O}_2$, is exothermic and can produce O_2 in both its ground state ($\tilde{X}^3\Sigma_g^-$) and its first excited state ($\tilde{a}^1\Delta_g$). As a result, this reaction can proceed on both a singlet and a triplet potential energy surface.

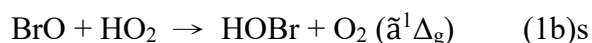
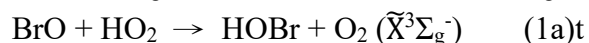
Recently, Tsona, Tang and Du published a paper entitled “Impact of water on the $\text{BrO} + \text{HO}_2$ gas-phase reaction: mechanism, kinetics and products” (Phys Chem Chem Phys 2019, 21, 20296-203072). The results of this work showed significant differences from those published earlier on this reaction by Chow et al. (Phys Chem Chem Phys 2016, 18, 30554-30569). Further calculations performed in this present work, combined with higher level calculations published by Chow et al. (Phys Chem Chem Phys 2016, 18, 30554-30569), demonstrate that the work of Tsona et al. is flawed because the integration grid size used in their lowest singlet and triplet calculations is too small, and a closed-shell wavefunction, rather than an open-shell wavefunction, has been used for the singlet surface. The major conclusion in the work of Tsona et al. that the lowest singlet and triplet channels are barrierless is shown to be incorrect.

Also, the computed rate coefficients of Tsona et al. showed a positive temperature dependence, which is inconsistent with the experimentally observed negative temperature dependence, whereas the singlet rate coefficients computed by Chow et al. (Phys Chem Chem Phys 2016, 18, 30554-30569) showed a negative temperature dependence consistent with experiment.

Introduction

In a recent paper Tsona et al. reported a computational study on $\text{BrO} + \text{HO}_2 \rightarrow \text{HOBr} + \text{O}_2$ prior to studying the effect of water on this reaction computationally (1). This work shows a number of significant differences from an earlier study we made of this reaction (2). We highlight these differences and discuss their likely origins in this Comment. Figures 1 and 2, taken from Figure 1 of reference (1) and Figure 1 of reference (2), allow this comparison to be made easily. They show computed schematic pathways in the work of Tsona et al.(1) and Chow et al.(2) respectively. The atmospheric importance of the $\text{BrO} + \text{HO}_2$ reaction and the experimental rate coefficient (k) measurements, which show a negative temperature dependence of k , are summarized in the Supplementary Information (SI) section (3-14)

Our work, Chow et al. (2), has shown that of the possible reaction channels i.e. (1) $\text{BrO} + \text{HO}_2 \rightarrow \text{HOBr} + \text{O}_2$, (2) $\text{BrO} + \text{HO}_2 \rightarrow \text{HBr} + \text{O}_3$, (3) $\text{BrO} + \text{HO}_2 \rightarrow \text{OBrO} + \text{OH}$, (4) $\text{BrO} + \text{HO}_2 \rightarrow \text{BrOO} + \text{OH}$, (1) has the lowest activation energies and is the major contributor to the overall rate coefficient at temperatures relevant to the troposphere. It is important to note, however, that reaction (1) can occur on two surfaces, a singlet and a triplet surface, as O_2 can be produced in either its ground state ($\tilde{\text{X}}^3\Sigma_g^-$) or its first excited state ($\tilde{\text{a}}^1\Delta_g$). These two channels are



The labelling, of (1a) and (1b), follows reference (2) with the letters “t” and “s” being added for clarity. Use of available standard heats of formation shows that both reactions are exothermic with reaction (1a)t being more exothermic than (1b)s by $\sim 22.5 \text{ kcal.mol}^{-1}$.

Comparison of the work of Tsona et al.(1) and our work (Chow et al. (2)) immediately shows a number of differences. First of all, the computed rate coefficients of Tsona et al.(1) show a positive temperature dependence (see Table S2 of the SI of ref.(1)) whereas those of ref.(2) show a negative temperature dependence, as observed experimentally. Also, in ref.(1) the lowest singlet and triplet surfaces were computed to be barrierless (no transition states (TSs) were found in these calculations for these lowest pathways) and they were therefore expected to contribute equally to the overall rate coefficient. In contrast, in our work (ref.(2)), TSs were located in both the lowest singlet and triplet channels, with the singlet channel ((1b)s) computed to have a lower activation energy than the triplet channel ((1a)t). The triplet channel was computed to have a TS ΔE of $2.58 \text{ kcal.mol}^{-1}$ whereas the singlet channel was computed to have a TS ΔE as $-3.05 \text{ kcal.mol}^{-1}$ at the highest level used (see Tables 1 and 2 of ref.(2)), and therefore the singlet channel was computed to make the dominant contribution to the overall rate coefficient in the temperature range considered. In order to understand the reasons for these differences, the methods used in refs (1) and (2), and the key parts of the potential energy surfaces obtained, need to be investigated and compared. The schematic potential energy diagrams are shown in Figures 1 and 2. Figure 1 is Figure 1 of Tsona et al.(1), with the pathway for channel (2) removed, and Figure 2 is Figure 1 of ref.(2), without the parts which refer to channels (2), (3) and (4)) i.e. for ease of comparison they both only refer to channels (1a)t and (1b)s.

Figure 1

Figure 2

Computational Details

These are given in the original papers (1,2), so only a summary of the methods used is given here.

Tsona et al.(1)

The M06-2X density functional was used with aug-cc-pVDZ basis sets to search for stationary points on the triplet and singlet potential energy surfaces. Once stationary points were located, relative energies were improved by performing single point calculations at the M06-2X/AVDZ optimised geometries at the CCSD(T) level with aug-cc-pVTZ basis sets. i.e. CCSD(T)/AVTZ//M06-2X/aug-cc-pVDZ calculations were carried out. All these electronic structure calculations were carried out using GAUSSIAN09 (15). It appears that the default parameters were used in these calculations. In particular, it seems that the default integration grid (specified as “INTEGRAL= FINEGRID”; this is referred to as the “small grid” in this work) was used. Evidence for this is presented later. The default integration grid used in GAUSSIAN09 was developed for, and refined on, earlier generations of functionals than the M06-2X functional and similar functionals. It has been demonstrated that when the M06-2X functional and similar hybrid meta exchange-correlation functionals are used, larger integration grids should be used than the default grid, as use of a default grid in codes such as GAUSSIAN with M06-2X can give rise to errors such as inaccurate binding energies and geometries, and inability to locate transition states in weakly bound systems (16-19). This problem has been traced to the kinetic energy density enhancement factor utilized in the exchange component of the M06-2X functional (16,17). For this reason, a larger integration grid (specified by “INTEGRAL= ULTRAFINE”; this is referred to as the “large grid” in this work) than the default grid was used for all the GAUSSIAN calculations reported by Chow et al in ref.(2).

To calculate rate coefficients a two transition-state (TS) approach was used by Tsona et al.(1), which is appropriate for reactions with low-lying or negative barriers. This two TS approach involves two TS bottlenecks for the overall reaction. The first bottleneck, at the outer TS, occurs on association of the two reactants, where they need to overcome a centrifugal barrier to form the reactant complex (RC), and the second bottleneck, at the inner TS, is at the TS which separates the RC from the product complex (PC).

The overall rate coefficient (k) is given, according to this theory, as:-

$$\frac{1}{k} = \frac{1}{k_{in}} + \frac{1}{k_{out}} \quad \text{-----} \quad (1)$$

where k_{in} and k_{out} are inner and outer rate coefficients which can be calculated by transition state theory (TST) and phase space theory (PST) respectively. In the work of Tsona et al. (1), k_{out} was calculated using classical PST as evaluated by equ.(2)

$$k_{out} = 2^{\frac{11}{6}} \Gamma\left(\frac{2}{3}\right) \sqrt{\frac{\pi}{\mu}} C^{\frac{1}{3}} (k_B T)^{\frac{1}{6}} K_v \quad \text{-----} \quad (2)$$

The terms in this expression are as defined in ref.(1). However, it should be noted that K_v is a correction factor to correct a rate coefficient of a barrierless reaction to give a good fit to an experimental value. Setting K_v to unity recovers the computed rate coefficients at the classical PST level.

For the lowest triplet and singlet surfaces, the value of K_v used in ref.(1) was 6.1 which was chosen to give the best agreement with available experimental rate coefficients. (This value of K_v was obtained with $v=4/7$ in equ.(7) in ref.(1)). Using this value of K_v , the rate coefficients for the lowest singlet and triplet surfaces, which were both computed to be barrierless in ref.(1), were both obtained as $2.21 \times 10^{-11} \text{ cm}^3 \cdot \text{molecule}^{-1} \text{s}^{-1}$. Inspection of equation (2) shows that this approach will give a $T^{1/6}$ dependence for k_{out} . In the absence of an inner TS, (a “barrierless reaction”) $k = k_{out}$.

Chow et al.(2)

As in ref.(1), M06-2X/AVDZ geometry optimizations and IRC searches were carried out in ref.(2) using GAUSSIAN09, but with a large integration grid (specified by “INTEGRAL=ULTRAFINE” as discussed above). The relative energies of stationary points obtained were then improved by fixed point calculations using higher level *ab initio* methods. Initially, the RHF/UCCSD(T) method as implemented in MOLPRO (20) was used with the aug-cc-pVXZ (for H, C and O) and aug-cc-pVXZ-PP (for Br) basis sets, where $X = T$ or Q . Extrapolation to the complete basis set (CBS) limit of computed relative electronic energies obtained with the AVQZ and AVTZ basis sets was carried out employing the $1/X^3$ formula. However, for the TS of channel (1a)t, although the CCSD iterations in the UCCSD(T) calculations converged, the computed T_1 diagnostic value was rather large (~ 0.1), suggesting non-negligible multireference (MR) character. In order to circumvent this problem, Brueckner theory was employed, as with Brueckner doubles (BD) the T_1 value is zero. BD(T)/AVQZ and BD(TQ)/AVTZ single energy calculations were carried out as implemented in GAUSSIAN09 (15). Computed relative BD(T) energies obtained using the AVQZ and AVTZ basis sets were extrapolated to the CBS limit employing the $1/X^3$ formula. The highest level of relative electronic energies obtained in the present study is BD(TQ)/CBS, which combines the BD(T)/CBS value with the (Q) contribution from the $\{\text{BD(TQ)} - \text{BD(T)}\}$ relative energies.

For the triplet channel (1a)t, for reasons outlined in ref.(2), BD/AVDZ geometry optimizations, and subsequent frequency calculations, were carried out on the TS but not the RC and PC.

Consequently, for the RC and PC, the best computed relative energies are at the CCSD(T)/CBS//M06-2X/AVDZ level, while for the TS the best computed ΔE is at the BD(TQ)/CBS//BD/AVDZ level.

For the singlet channel, (1b)s, it was important to use a wavefunction for an open-shell singlet state in order to treat adequately the change in the potential energy surface from the TS backwards to the RC and on to the reagents, two molecular radicals, as well as the change from the TS forwards to the products. It is well known that if a single determinantal restricted wavefunction is used for H_2 , to investigate the process $H_2 \rightarrow H + H$, then incorrect dissociation is obtained to a “state” which is combination of neutral ($H + H$) and ionic ($H^+ + H^-$) contributions, and, as a result, the dissociation energy is overestimated. Therefore, for the singlet channel (1b)s, unrestricted wavefunctions were used, together with guess=mix in GAUSSIAN09, in order to obtain an open-shell singlet state which can correctly describe movement from the TS forwards to the products, and backwards from the TS to the open-shell reactants.

UCCSD(T)/AVnZ//M06-2X/AVDZ calculations, summarised in our work, ref.(2), and the associated SI, indicate that MR character is only significant for the TS of the triplet surface with a T_1 value of 0.1. For the other stationary points on the singlet and triplet surfaces the T_1 value is much lower than this. Hence for the triplet TS, CASSCF/AVDZ calculations were carried out at the M06-2X/AVDZ geometry. Inspection of the CI coefficients obtained from these CASSCF calculations, performed with different active electrons and active spaces, show that the MR character is not very large for the triplet TS and in this connection BD methods are expected to be adequate (see the SI section of ref.(2)). For the singlet TS, the CASSCF(2,4)/NEVPT2 results are adequate as the CASSCF(2,4) wavefunction has accounted for the two-configurational open-shell singlet wavefunction (see SI section of ref.(2)). The excellent agreement between the CASSCF/NEVPT2/CBS and BD(TQ)/CBS TS relative energies reinforces this conclusion.

To calculate rate coefficients from the computed potential surfaces, use was made of equation (1). k_{in} was calculated by a number of methods with the highest level method being ICVT/SCT using POLYRATE (21). k_{out} was calculated using quantum PST where the microcanonical number of states was evaluated according to equ.(2) in reference (22).

Also, as outlined in ref.(2), a correction was made for spin-orbit splitting in the ground state of BrO, in the evaluation of all relative energies (+1.394 kcal mol⁻¹ was added to all ΔE values to make this correction), and the two spin-orbit states of BrO were included in all rate coefficient calculations.

The characteristics of the electronic structure methods used in this work and refs.(1,2) are given in the SI section.

Table 1

Calculated relative energies, relative enthalpies at 298 K, and relative Gibbs free energies at 298 K for the Triplet Channel $\text{BrO} + \text{HO}_2 \rightarrow \text{HOBr} + \text{O}_2 (\tilde{\text{X}}^3\Sigma_g^-)$
(kcal.mol⁻¹)

Level Relative energies	CCSD(T)/AVTZ// M06-2X/AVDZ (ref.(1)Tsona et al.)*	CCSD(T)/AVTZ// M06-2X/AVDZ This work, using the geometries given in the ESI of ref.(1)*	M06-2X/AVDZ This work, using the geometries given in the ESI of ref.(1)* using GAUSSIAN09 with a small integration grid (large grid values are in brackets) (see text)	M06- 2X/AVDZ Ref.(2) ^(a)	Higher level values Ref.(2) ^(a)
ΔE^{PCt1}	-49.45	-50.76	-53.68 (-53.68)	-52.26	-49.62
ΔE^{RX}		-48.89	-52.25 (-51.93)	-50.89	-47.96
ΔH^{PCt1}	-48.00	-49.91	-52.84 (-52.84)		
$\Delta H^{\text{RX}}_{298\text{K}}$		-48.38	-51.75 (-51.43)	-50.4	-47.5
ΔG^{PCt1}	-41.01	-42.52	-45.44 (-45.44)		
$\Delta G^{\text{RX}}_{298\text{K}}$		-47.75	-51.11 (-50.79)		

*no allowance has been made for the spin-orbit correction in BrO

(a) with spin-orbit correction in BrO (+1.39 kcal.mol⁻¹)

Table 2

Calculated relative energies, relative enthalpies at 298 K, and relative Gibbs free energies at 298 K for the Singlet Channel $\text{BrO} + \text{HO}_2 \rightarrow \text{HOBr} + \text{O}_2$ ($\tilde{a}^1\Delta_g$)

(kcal.mol⁻¹)

Level	CCSD(T)/AVTZ// M06-2X/AVDZ (ref.(1)Tsona et al.)*	CCSD(T)/AVTZ// M06-2X/AVDZ This work, using the geometries given in the ESI of ref.(1)*	M06-2X/AVDZ This work, using the geometries given in the ESI of ref.(1)* using GAUSSIAN09 with a small integration grid (large grid values are in brackets (see text)	M06- 2X/AVDZ Ref.(2) ^(a)	Higher level values Ref.(2) ^(a)
ΔE^{RCs1}	-6.88	-9.08	-0.0034 (-0.69)	-5.07	-4.03
ΔE^{TSs1}	-2.65	-2.31	5.51 (5.51)	-3.50	-3.05
ΔE^{PCs1}	-20.28	-21.78	-17.65 (-17.59)		
ΔE^{RX}	-26.29	-26.39	-29.75 (-29.43)	-36.81	-25.53
ΔH^{RCs1}	-5.40	-7.62	1.42 (0.78)		
ΔH^{TSs1}	-4.27	-3.97	3.84 (3.84)		
ΔH^{PCs1}	-18.78	-20.93	-17.65 (-16.78)		
$\Delta H^{\text{RX}}_{298\text{K}}$	-25.80	-25.89	-29.25 (-28.93)		-25.0
ΔG^{RCs1}	4.95	2.73	11.77 (11.12)		
ΔG^{TSs1}	7.51	7.88	15.69 (15.69)		
ΔG^{PCs1}	-11.30	-12.93	-8.82 (-8.86)		
$\Delta G^{\text{RX}}_{298\text{K}}$	-25.17	-25.25	-28.61 (-28.61)		

*no allowance has been made for the spin-orbit correction in BrO

(a) with spin-orbit correction in BrO (+1.39 kcal.mol⁻¹)

Results and Discussion

Figures 1 and 2 provide a useful starting point for discussion of the work reported in refs (1) and (2). Figure 1, from ref.(1), shows a graph of free energy change, ΔG , vs reaction coordinate, whereas Figure 2, from ref.(2), shows relative energy changes, ΔE , vs reaction coordinate. Inspection of these figures shows that a number of stationary points seen in Figure 2 are not present in Figure 1. As shown in Figure 1, Tsona et al.(1) found two singlet channels:- a barrierless singlet channel to PC_{s1} and a singlet channel with a barrier, via RC_{s1} and TS_{s1}, to PC_{s1}, although no details are given in their work about how these different channels were obtained. They also found a barrierless triplet channel to PC_{t1}. As shown in Figure 2, Chow et al.(2) found a reaction complex, a TS and a product complex for the triplet channel (RC_t (RC1a), TS_t (TS1a) and PC_t (PC1a) in Figure 2) and a reaction complex and a TS for the singlet channel (RC_s (RC1b) and TS_s (TS1b) in Figure 2) but a product complex was not located for this channel in ref.(2).

As Tsona et al. (1) report the M06-2X/AVDZ computed geometries of the stationary points shown in Figure 1 in the SI of ref.(1), it was decided to use these geometries to check the relative energies quoted in their work. These calculations were fixed point CCSD(T)/AVTZ//M06-2X/AVDZ calculations with GAUSSIAN09 with the default integration grid size. The relative energies of singlet stationary points were computed at the CCSD(T)/AVTZ//RM06-2X/AVDZ level, using restricted M06-2X wavefunctions to treat singlet species.

The results are shown in Table 1 for the triplet channel and Table 2 for the singlet channel. In Table 1, the reaction energies, ΔE , reaction enthalpies, ΔH , and free energies, ΔG , agree reasonably well with those of Tsona et al (1). In Table 2, the relative energies of TS_{s1} and PC_{s1} agree reasonably well with the values of Tsona et al.(1) except that the relative energy of RC_{s1} (-9.08 kcal.mol⁻¹) differs from the quoted value of Tsona (-6.88 kcal.mol⁻¹).

The results shown in Table 1 are as follows:- column 2 shows the CCSD(T)/AVTZ//M06-2X/AVDZ values published by Tsona et al. (1), column 3 shows the CCSD(T)/AVTZ//M06-2X/AVDZ results obtained in this present work using Tsona's published geometries, column 4 shows the M06-2X values obtained in this present work using Tsona's geometries with default input parameters including a small integration grid, column 5 lists the relative energies obtained by Chow et al. (2) at the M06-2X/AVDZ level, after geometry optimisation using a large integration grid, and column 6 shows the higher level ΔE values quoted by Chow in ref.(2).

Considering the triplet channel(1a)t first, although the relative energy of PC_{t1} obtained in this present work (-50.76 kcal.mol⁻¹) is very close to that obtained by Tsona et al.(1) (-49.45 kcal.mol⁻¹) with fixed point calculations using the same geometry and the default (small) integration grid, a slightly different optimized geometry was obtained by Chow et al. in ref.(2), using a larger integration grid, compared to that of ref.(1). The main difference was the orientation of the O-O unit in O₂ relative to HOBr in the product complex. Starting with the optimized geometry of TS_t (TS1a) from the original work of Chow et al.(2) (obtained with a large integration grid), it was found that performing a TS search with this structure with a default (small) grid failed to locate the TS.

Similarly, optimizing the RCt structure in ref.(2) with a default grid led directly to PCt. However, when the larger grid was used the stationary points RCt, TSt, and PCt, found in ref.(2), could all be located. Clearly, in the triplet channel the potential in the TS region is very shallow and the fact that the stationary points RCt, and TSt, located in ref.(2) could not be found in the work of Tsona et al.(1), is an error caused by the use of too small a grid size in ref.(1).

Table 2 summarises the relative energies, enthalpies and free energies at 298 K for the singlet channel, as is done in Table 1 for the triplet channel. As for the triplet channel, a large grid size should be used for the singlet channel, and, as already discussed, an open-shell singlet wavefunction should also be used (obtained with guess=mix in GAUSSIAN09) (as has been done by Chow et al. in ref.(2)). The results of calculations performed in this present work indicate that the singlet calculations reported in ref.(1) were carried out with a default (small) grid size and a closed shell singlet wavefunction. The evidence is as follows:-

(a) Using the geometry of TSs1 provided by Tsona et al.(1), fixed point calculations using a closed-shell wavefunction and a default (small) grid-size at the M06-2X/AVDZ and CCSD(T)/AVTZ//M06-2X/AVDZ levels gave ΔE values very close to those of Tsona et al.(1) (see Table 2). If a TS search is carried out at the RM06-2X/AVDZ level starting with the geometry of Tsona et al. (1) of TSs1 using the default (small) grid and a closed shell wavefunction, then a TS can be located which is very similar to TSs1 of Tsona et al. (1). If this TS search is repeated using an open-shell singlet wavefunction, the TS cannot be located. However, if this TS search is repeated with a open-shell singlet wavefunction and a larger grid, the transition state TS found by Chow et al. in ref.(2) was obtained.

In order to show that closed-shell singlet wavefunctions are inappropriate for the separate reactants ($\text{BrO} + \text{HO}_2$) and RC1s, the following calculations were carried out:-

(b) For RCs1, partial optimization of the BrO and HO_2 fragments in $\text{BrO} \cdots \text{HO}_2$ was carried out at an inter-fragment distance of 50 Å at the unrestricted M06-2X/AVDZ level (using guess=mix in GAUSSIAN09) with a large integration grid. Each fragment was found to be neutral with one of the two unpaired electrons localized on BrO and the other localised on HO_2 . The energy relative to the reactants, ΔE , was computed as 0.0053 kcal.mol⁻¹. The HOMO (containing 1 electron) is almost completely localized on BrO, which is reasonable. However, if this calculation is repeated using a restricted closed-shell wavefunction with the default (small) grid-size, the computed relative energy is 87.98 kcal.mol⁻¹ and the HOMO is delocalised over the whole of $\text{BrO} \cdots \text{HO}_2$. The same result is obtained when this calculation is repeated with a restricted closed-shell wavefunction but a larger grid size.

(c) Using the geometry of RCs1 given by Tsona et al.(1) to do geometry optimization with an open shell wavefunction (i.e. start the optimization with guess=mix) and a large grid, the calculation converged to a closed-shell singlet (the spin-density was zero on each centre). A repeat of this calculation at the restricted M06-2X level with a closed-shell wavefunction and a large grid gave the same result. Also, using the geometry reported by Tsona et al.(1), fixed point calculations were

performed on RCs1 at the M06-2X/AVDZ and CCSD(T)/AVTZ//M06-2X/AVDZ levels. The ΔE value obtained at the CCSD(T)/AVTZ//M06-2X/AVDZ level ($-9.08 \text{ kcal.mol}^{-1}$) differed from that quoted by Tsona et al. ($-6.88 \text{ kcal.mol}^{-1}$) at the same level, in the SI of ref.(1). The reason for this difference is not known, as no M06-2X/AVDZ values are given in ref.(1). However, as an optimized geometry of RCs1 can be obtained at the restricted M06-2X/AVDZ level which is very close to that given in ref.(1), the problem may lie in the higher level CCSD(T)/AVTZ calculations performed in ref.(1).

In summary, the main results from this investigation of the work of Tsona et al.(1) are:-

- (1) For the triplet surface, when we repeated the TS search using the default small integration grid, no TS could be found. However, when the larger integration grid was used the TS could be located, as in our earlier work (2). Since the triplet potential in the region of the TS was shown to be rather flat in our previous work (2), it is clear that the integration grid size is very important in locating the triplet TS.
- (2) For the singlet surface with a barrier at TSs1, when we repeated M06-2X calculations using closed-shell singlet wavefunctions we obtained results which are very similar to those of Tsona et al.(1) except for RCs1 (see above). This indicates that Tsona et al.(1) have employed closed-shell wavefunctions in their M06-2X calculations on the singlet surface, which is clearly inappropriate.
- (3) Repeating M06-2X geometry optimization calculations on RCs1, followed by fixed point calculations at the CCSD(T)/AVTZ//M06-2X/AVDZ level, gave a computed relative energy which was significantly different from that of ref.(1) even though a very similar optimised geometry was used in both cases. The reason for this is not known as no M06-2X relative energies were quoted in ref.(1). The error is thought to arise in the higher level CCSD(T)/AVTZ calculations performed in ref.(1).
- (4) For the singlet channels obtained by Tsona et al.(1) at the M06-2X level, based on point (2) above, it can only be assumed that closed-shell singlet wavefunctions have been used in all the calculations on the singlet channels, including the barrierless pathway claimed in ref.(1). Based on points (1) and (2), we can only conclude that the result of Tsona et.(1) of a barrierless singlet channel is an error arising from use of an incorrect singlet wavefunction and too small an integration grid.
- (5) In ref.(1), the claimed good agreement between computed and experimental rate coefficients is questionable. Firstly, the “good agreement” is only at one temperature (298 K) and this was obtained using a fitting parameter ($K_v = 6.1$). Without this fitting factor, the computed rate coefficient doesn't agree with the experimental rate coefficient at 298 K, and at other temperatures relevant to the troposphere. Secondly, the temperature dependence computed by Tsona et al.(1) does not agree with the experimental temperature dependence. In ref.(1) a positive temperature dependence was computed whereas experimental evidence clearly shows a negative temperature dependence, as was calculated in our work (Chow et al.(2)).

Conclusions

For the singlet calculations reported by Tsona et al.(1), it appears that they have used a default (small) grid-size and closed-shell singlet wavefunctions with restricted M06-2X/AVDZ calculations. For the triplet calculations of Tsona et al.(1) a small grid size has been used. This has led to erroneous results as a larger grid-size should have been used for both the singlet and triplet channels, and an open-shell unrestricted wavefunction should have been used for the singlet channel. The test calculations performed in this work, and the results of higher level calculations in ref.(2), demonstrate that the schematic potential energy surfaces reported by Tsona et al. in ref.(1) are incorrect. As reported by Chow et al.(2) both the lowest singlet and triplet channels proceed via low-lying transition states and they are not barrierless as claimed by Tsona et al.(1). The triplet channel is the most exothermic but the singlet channel has the lowest activation energy and therefore has the highest rate coefficient. The flawed results for $\text{BrO} + \text{HO}_2$ reported in ref.(1) must mean that the computational results obtained for the effects of water on this reaction, and the conclusions drawn from these results, which are included in ref.(1), must also be questionable.

Acknowledgements

The authors are grateful to the Research Grant Council (RGC) of the Hong Kong Special Administrative Region (PolyU 153013/15P) and the Research Committee of the Hong Kong Polytechnic University (Grant No: YBNK and YBAV) for support of this work.

References

1. N. T. Tsona, S. Tang and L. Du Impact of water on the $\text{BrO} + \text{HO}_2$ gas-phase reaction: mechanism, kinetics and products Phys Chem Chem Phys 2019, **21**, 20296-20307
2. R. Chow, D. K. W. Mok, E. P. F. Lee and J. M. Dyke A theoretical study of the atmospherically important radical-radical reaction $\text{BrO} + \text{HO}_2$; the product channel $\text{O}_2(\text{a}^1\Delta_g) + \text{HOBr}$ is formed with the highest rate Phys Chem Chem Phys 2016, **18**, 30554-30569
3. R. A. Cox and D. W. Sheppard, Rate coefficient for the reaction $\text{BrO} + \text{HO}_2$ at 303 K, J. Chem. Soc., Faraday Trans.2, 1982, **78**, 1383–1389.
4. R. Atkinson, D. L. Baulch, R. A. Cox, J. N. Crowley and J. N. Hampson, et al., Evaluated kinetic and photochemical data for atmospheric chemistry Vol. III Gas-phase reactions of inorganic halogens, Atmos. Chem. Phys., 2007, **7**, 981–1191.
5. W. J. Bloss, D. Rowley, R. A. Cox and R. L. Jones, Rate coefficient for the $\text{BrO} + \text{HO}_2$ reaction at 298 K, Phys. Chem. Chem. Phys., 2002, **4**, 3639–3647.
6. V. Bedjanian, V. Riffault and G. Poulet, Kinetic study of the reactions of BrO radicals with HO_2 and DO_2 , J. Phys. Chem. A, 2001, **105**, 3167–3175.

7. J. M. Cronkite, R. E. Stickel, J. M. Nicovich and P. H. Wine, Laser flash photolytic studies of radical–radical reaction kinetics: the BrO + HO₂ reaction, *J. Phys. Chem. A*, 1998, **102**, 6651–6658.
8. Z. Li, R. R. Friedl and S. P. Sander, Kinetics of the HO₂ + BrO reaction over the temperature range 233–348 K, *J. Chem. Soc., Faraday Trans.*, 1997, **93**, 2683–2691.
9. M. Larichev, F. Maguin, G. Le Bras and G. Poulet, Kinetics and mechanism of the BrO + HO₂ reaction, *J. Phys. Chem.*, 1995, **99**, 15911–15918.
10. G. Poulet, M. Pirre, F. Maguin, R. Ramaroson and G. Le Bras, Role of the BrO + HO₂ reaction in the stratospheric chemistry of bromine, *Geophys. Res. Lett.*, 1992, **19**, 2305–2308.
11. A. Mellouki, R. K. Talukdar and C. J. Howard, Kinetics of the reactions of HBr with O₃ and HO₂: the yield of HBr from HO₂ + BrO, *J. Geophys. Res.*, 1994, **99**, 22949–22954.
12. I. Bridier, B. Veyret and R. Lesclaux, Flash photolysis kinetic study of reactions of the BrO radical with BrO and HO₂, *Chem. Phys. Lett.*, 1993, **201**, 563–568.
13. M. J. Elrod, R. F. Meads, J. B. Lipson, J. V. Seeley and M. J. Molina, Temperature dependence of the rate constant for the HO₂ + BrO reaction, *J. Phys. Chem.*, 1996, **100**, 5808–5812.
14. M.K.M.Ward and D.M.Rowley Kinetics of the BrO + HO₂ reaction over the temperature range T= 246-314 K *Phys Chem Chem Phys* 2017, **19**, 23345-23356
15. M. J. Frisch; G. W. Trucks; H. B. Schlegel; G. E. Scuseria; M. A. Robb; J. R. Cheeseman; G. Scalmani; V. Barone; B. Mennucci; G. A. Petersson; H. Nakatsuji; M. Caricato; X. Li; H. P. Hratchian; A. F. Izmaylov; J. Bloino; G. Zheng; J. L. Sonnenberg; M. Hada; M. Ehara; K. Toyota; R. Fukuda; J. Hasegawa; M. Ishida; T. Nakajima; Y. Honda; O. Kitao; H. Nakai; T. Vreven; J. A. Montgomery, Jr.; J. E. Peralta; F. Ogliaro; M. Bearpark; J. J. Heyd; E. Brothers; K. N. Kudin; V. N. Staroverov; T. Keith; R. Kobayashi; J. Normand; K. Raghavachari; A. Rendell; J. C. Burant; S. S. Iyengar; J. Tomasi; M. Cossi; N. Rega; J. M. Millam; M. Klene; J. E. Knox; J. B. Cross; V. Bakken; C. Adamo; J. Jaramillo; R. Gomperts; R. E. Stratmann; O. Yazyev; A. J. Austin; R. Cammi; C. Pomelli; J. W. Ochterski; R. L. Martin; K. Morokuma; V. G. Zakrzewski; G. A. Voth; P. Salvador; J. J. Dannenberg; S. Dapprich; A. D. Daniels; O. Farkas; J. B. Foresman; J. V. Ortiz; J. Cioslowski and D. J. Fox, *Gaussian 09; Revision E.01*, Gaussian, Inc., Wallingford, CT, 2013.
16. N. Mardirossian and M.H. Head-Gordon Thirty years of density functional theory in computational chemistry: an overview *Molecular Physics* 2017, **19**, 2315-2372
17. S.E . Wheeler and K.N.Houk Integration Grid Errors for Met-GGA- Predicted Reaction Energies: Origin of Grid Errors for the M06 Suite of Functionals *J.Chem Theory Comput* 2010, **6**, 395-404
- 18.I.D.Mackie and G.A.DiLabio Accurate dispersion interactions from standard density functional theory methods with small basis sets *Phys Chem Chem Phys* 2010, **12**, 6092-6098

19. Y. Zhang, N. Ma and W. Wang Assessment of the Performance of the M05-Class and M06-Class Functionals for the Structure and Geometry of the Hydrogen-Bonded and Halogen-Bonded Complexes J Theoretical and Computational Chemistry 2012, **11**, 1165-1173
20. H.-J. Werner, P. J. Knowles, G. Knizia, F. R. Manby, M. Schütz, P. Celani, T. Korona, R. Lindh, A. Mitrushenkov, G. Rauhut, K. R. Shamasundar, T. B. Adler, R. D. Amos, A. Bernhardsson, A. Berning, D. L. Cooper, M. J. O. Deegan, A. J. Dobbyn, F. Eckert, E. Goll, C. Hampel, A. Hesselmann, G. Hetzer, T. Hrenar, G. Jansen, C. Köppl, Y. Liu, A. W. Lloyd, R. A. Mata, A. J. May, S. J. McNicholas, W. Meyer, M. E. Mura, A. Nicklass, D. P. O'Neill, P. Palmieri, D. Peng, K. Pflüger, R. Pitzer, M. Reiher, T. Shiozaki, H. Stoll, A. J. Stone, R. Tarroni, T. Thorsteinsson, and M. Wang, MOLPRO, version 2012.1, a package of ab initio programs, 2012, see <http://www.molpro.net>.
21. J. Zheng, S. Zhang, B. J. Lynch, J. C. Corchado, Y. Y. Chuang, P. L. Fast, W. P. Hu, Y. P. Liu, G. C. Lynch, K. A. Nguyen, et al., POLYRATE version 2010-A (June, 2010), Copyright 1988–2010 D. G. Truhlar and Regents of the University of Minnesota, Minneapolis, Minnesota, USA.
22. S. North and G. E. Hall Quantum phase space theory for the calculation of v-j vector correlations J. Chem Phys 1996, **104**, 1864-1874

Figure Captions

Figure 1

A schematic potential energy diagram taken from ref.(1) for the Triplet $\text{BrO} + \text{HO}_2 \rightarrow \text{HOBr} + \text{O}_2$ ($\tilde{\text{X}}^3\Sigma_g^-$) and Singlet $\text{BrO} + \text{HO}_2 \rightarrow \text{HOBr} + \text{O}_2$ ($\tilde{\text{a}}^1\Delta_g$) reactions. Relative free energies, ΔG (in kcal.mol⁻¹), were calculated in ref.(1) at the CCSD(T)/AVTZ//M06-2X/AVDZ level. This figure is the same as Figure 1 of ref.(1), but with the pathway for $\text{BrO} + \text{HO}_2 \rightarrow \text{HBr} + \text{O}_3$ removed and the ΔG values added from Table 1 of ref.(1).

Figure 2

A schematic potential energy diagram taken from ref.(2) for the Triplet $\text{BrO} + \text{HO}_2 \rightarrow \text{HOBr} + \text{O}_2$ ($\tilde{\text{X}}^3\Sigma_g^-$) and Singlet $\text{BrO} + \text{HO}_2 \rightarrow \text{HOBr} + \text{O}_2$ ($\tilde{\text{a}}^1\Delta_g$) reactions. This figure is the same as Figure 1 of ref.(2), except that the pathways for reactions (2),(3) and (4) have been removed. Stationary points are shown with their relative electronic energies, ΔE (in kcal.mol⁻¹), with zero-point correction at 0 K at the BD(TQ)/CBS level (incl. spin-orbit correction for BrO) in brackets

Supplementary Information

(a) Atmospheric Importance and summary of available rate coefficient measurements

The BrO + HO₂ reaction is important in the earth's atmosphere as it can lead to enhanced destruction of ozone. This occurs through production of HOBr, which can then undergo photolysis followed by reactions of the radicals produced (OH and Br) with ozone. It is clearly important to establish the mechanism of the BrO + HO₂ reaction and determine its rate coefficient at temperatures which are relevant to the troposphere (typically 220-320 K). Experimentally the rate coefficient of this reaction has been measured at different temperatures in this temperature range by a number of research groups (3-14) and they show that the rate coefficient decreases as the temperature increases i.e. a negative temperature dependence is observed. The most recent rate coefficient determinations were made by Ward and Rowley (14). They obtained rate coefficients of $(2.55 \pm 0.33) \times 10^{-11}$, $(2.89 \pm 0.31) \times 10^{-11}$ and $(3.7 \pm 1.5) \times 10^{-11}$ cm³. molecule⁻¹s⁻¹ at 314.1, 298.1 and 246.1 K respectively.

(b) The characteristics of the electronic structure methods used in this work and refs.(1,2).

(i) DFT calculations with the M06-2X functional

The overall strategy used is to obtain the geometries and harmonic vibrational frequencies of the stationary points of a reaction (reactants, RC, TS, PC and products) on the potential energy surface using DFT calculations with the M06-2X functional, as well as their energies relative to the reactants. As described in ref.(2), the M06-2X functional was chosen because it has been shown to perform well for TS structures and reaction barrier heights in a number of benchmark studies. The M06-2X is a meta exchange-correlation functional and it has been demonstrated that, when a functional of this type is used with codes such as GAUSSIAN, larger integration grids should be used rather than the smaller default grids. Use of default grids can give rise to inaccurate binding energies and geometries, and the inability to locate transition states in weakly bound systems (16-19).

(ii) CCSD(T) calculations

CCSD(T)/AVTZ calculations at M06-2X/AVDZ optimised geometries have been performed in refs.(1) and (2). CCSD(T) means coupled cluster (CC) with a full treatment of single (S) and double (D) excitations. An estimate of the connected triples (T) excitations is calculated non-iteratively via many body perturbation theory. The central postulate of CC theory is that the full CI wavefunction can be described by a cluster operator (e^T) acting on a Hartree-Fock (HF) wavefunction. For CCSD calculations the cluster operator only includes single and double excitations. The CCSD(T) method relies on the HF wavefunction being the dominant determinant (i.e. the method is based on a single determinant being a reasonable approximation to the true wavefunction). One test of multireference character (MR) that is often used is to calculate the T_1 diagnostic of Lee and Taylor. If T_1 is too large (typically > 0.04) then results of CCSD(T) calculations should be treated with caution.

For the CCSD(T)/AVTZ//M06-2X/aug-cc-pVDZ calculations reported by Tsona et al. in ref(1)

no T_1 values were reported.

In the work of Chow et al.(2) UCCSD(T)/AVnZ//M06-2X/AVDZ calculations indicate that MR character is only significant for the TS of the triplet surface with a T_1 value of 0.1. For the other stationary points on the singlet and triplet surfaces the T_1 value is much lower than this. Hence for the triplet TS, CASSCF/AVDZ calculations were carried out at the M06-2X/AVDZ geometry.

(iii) CASSCF calculations

In ref.(2) CASSCF/AVDZ calculations were carried out at M06-2X/AVDZ optimised geometries. The complete active space self-consistent field (CASSCF) is a specific type of MCSCF method in which the number of determinants or CSFs used in the expansion of the CI vector are defined by dividing the orbitals into three subspaces. In the first subspace, the *inactive space*, all orbitals are doubly occupied. The second subspace is known as the *active space*, and within this orbital space, a full-CI expansion is considered. The orbitals selected for the active space are those that contribute most to the multireference character of the particular system studied. Finally, the third subspace, known as the *virtual space*, consists of orbitals that are kept unoccupied. This method decreases the number of determinants or CSFs in the CI expansion since it limits the MC wave function within a specific subset of electrons and orbitals rather than treating all electrons in all orbitals as one would do in a traditional MRCI calculation. As such, the CASSCF method cannot be considered merely as a “black box” method, as *a priori* knowledge of the chemical system under study is needed for the proper choice of the active orbitals. A limitation of CASSCF is the number of electrons and orbitals that can be included in the active space, since the CI expansion increases exponentially with respect to the number of electrons and orbitals.

A CASSCF calculation for a given choice of active space and an active electrons will include some non-dynamic electron correlation. A second order perturbation theory calculation (CASPT2 or NEVPT2 (NEVPT stands for N-Electron Valence State Perturbation Theory)) can then be used to calculate the dynamic correlation energy contribution to the total energy.

For the triplet TS, CASSCF/AVDZ calculations were carried out at the M06-2X/AVDZ geometry (2). Inspection of the CI coefficients obtained from these CASSCF calculations, performed with different active electrons and active spaces, show that the MR character is not very large for the triplet TS and in this connection BD methods (see later) are expected to be adequate. For the singlet TS, the CASSCF(2,4)/NEVPT2 results are adequate as the CASSCF(2,4) wavefunction has accounted for the two-configurational open-shell singlet wavefunction. The excellent agreement between the CASSCF/NEVPT2/CBS and BD(TQ)/CBS TS relative energies reinforces this conclusion. (In CASSCF(2,4) there are 2 active electrons in an active space of 4 orbitals).

(iv) BD Calculations

As outlined above, the CCSD method is based on a HF wavefunction. This may be problematic in some cases. In such cases, before resorting to a multireference approach (e.g. CASSCF), there is a variant of CCSD that has shown larger stability with respect to the choice of the reference function---the Brueckner doubles (BD) method. In this method, the BD reference function is built such that all the amplitudes for single excitations are zero. Starting from the initial reference (e.g. a HF single determinant), the orbitals are rotated until the above condition is satisfied. BD thus introduces an initial relaxation that is coupled with the CC expansion, which includes only double excitations. In many cases, BD provides a more reliable wavefunction than CCSD.

For the triplet TS, although the CCSD iterations in the UCCSD(T) calculations converged, the computed T_1 diagnostic value was rather large (~ 0.1), suggesting non-negligible multireference (MR) character. In order to circumvent this problem, Brueckner theory was employed, as with Brueckner doubles (BD) the T_1 value is zero. BD(T)/AVQZ and BD(TQ)/AVTZ single energy calculations were carried out. Computed relative BD(T) energies obtained using the AVQZ and AVTZ basis sets were extrapolated to the CBS limit employing the $1/X^3$ formula. The highest level of relative electronic energies obtained in the present study is BD(TQ)/CBS, which combines the BD(T)/CBS value with the (Q) contribution from the $\{\text{BD(TQ)}-\text{BD(T)}\}$ relative energies.